# Photohole Trapping Induced Platinum Cluster Nucleation on the Surface of TiO2 Nanoparticles

**ARTICLE** *in* THE JOURNAL OF PHYSICAL CHEMISTRY C · DECEMBER 2013

Impact Factor: 4.77 · DOI: 10.1021/jp410846k



**6 AUTHORS**, INCLUDING:

Jiwei Ma
Pierre and Marie Curie University - Paris 6
**23** PUBLICATIONS **160** CITATIONS
SEE PROFILE

Edgar Valenzuela
Autonomous University of Baja California
**13** PUBLICATIONS **94** CITATIONS
SEE PROFILE

Aurelien Habrioux
Université de Poitiers
**35** PUBLICATIONS **460** CITATIONS
SEE PROFILE

Nicolas Alonso-Vante
Université de Poitiers
**226** PUBLICATIONS **4,592** CITATIONS
SEE PROFILE

THE JOURNAL OF PHYSICAL CHEMISTRY C

Article

pubs.acs.org/JPCC

# Photohole Trapping Induced Platinum Cluster Nucleation on the Surface of $TiO_2$ Nanoparticles

Jiwei Ma, Edgar Valenzuela, Aldo S. Gago, Julie Rousseau, Aurélien Habrioux,* and Nicolas Alonso-Vante*

IC2MP, UMR-CNRS 7285, University of Poitiers, 4 rue Michel Brunet, 86022 Poitiers, France

**ABSTRACT:** The photocurrent response of $TiO_2$ nanoparticles synthesized via the sol−gel process was studied in the presence of methanol, ethanol, and isopropanol. The nanocrystalline nature of photoelectrodes showed an important photocurrent in the presence of alcohol following the order methanol ≈ ethanol > isopropanol > $H_2O$. This process mimics the photoelectrochemical response, and therefore a correlation of the photodeposition process of platinum nanoclusters on $TiO_2$ particles in the presence of alcohol molecules was devised. The photodeposition mechanism of platinum nanoislands at the surface of a nanocrystalline $TiO_2$ powder is discussed in the light of the photoelectrochemical results.

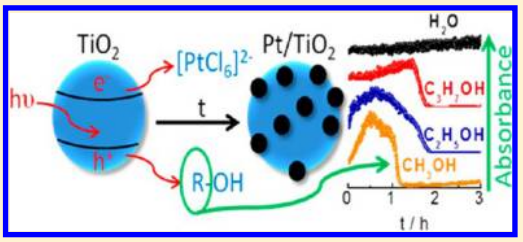


## 1. INTRODUCTION

Titanium dioxide is a promising material for environmental technologies due to its semiconducting properties, high resistance to corrosion, and low toxicity.[1] Nanocrystalline $TiO_2$ electrodes have been widely employed for applications such as solar energy conversion[2,3] or removal of organic pollutants in water.[4,5] It has also been used as substrate for catalytic materials in the heterogeneous catalysis.[6−8] In these applications, the tailoring of stable highly dispersed and efficient catalysts is currently a great challenge. This can be achieved by using $TiO_2$-based substrates.[9] Furthermore, the strength of the interaction between a substrate material (oxide, carbon) and a metallic catalyst can be greatly affected by the technique devised to perform the metal deposits on the support.[6,10] As an example, it is now well-known that the photodeposition technique[11] allows the formation of an interfacial alloy between the metal in the oxide and platinum nanoparticles,[7,12,13] responsible for improving the rate of electrochemical reactions such as oxygen reduction reaction[7] or CO oxidation.[14] This method simply consists in photoirradiating an aqueous solution containing the metallic precursor, titanium dioxide, and an organic molecule acting as a hole scavenger. The illumination of $TiO_2$ nanoparticles with UV light allows for the formation of electron−hole pairs that rapidly recombine after the photoexcitation event. Free charges can be also trapped by coordination defects at the surface of the nanoparticles and by lattice defects in the bulk material.[15] The generated electron−hole pairs are however capable of migrating or diffusing to the $TiO_2$ surface where they react with adsorbed molecules to achieve the reduction of the metallic precursor to metal clusters and the oxidation of hole scavengers. Although this method has been employed a long time ago to load noble metal nanoparticles on $TiO_2$ nanomaterial,[16−23] it is not fully understood, and there is a need for identifying and controlling the whole set of parameters that affect the size and the structural properties of photodeposited precious-metal-based nanoparticles. It is in fact essential to control these properties to design noble-metal-based catalytic nanomaterials since their activity depends on their chemical nature, morphology, crystallographic properties, and the position of the d-band center with respect to the Fermi level. Among the involved parameters, the effect of the chemical nature of the hole scavenger used, during the photodeposition process on the deposition rate of platinum nanoparticles on the surface of $TiO_2$ nanoclusters, has not been yet elucidated. That is why this study aims at bringing an improved understanding of the photodeposition of Pt nanoclusters onto nanoparticulated oxide anatase phase substrate in the presence of different alcohol molecules serving as hole scavenger. The effect of the alkyl chain length of the alcohol molecule on the photodeposition of platinum nanoparticles on $TiO_2$ will be described by coupling *in situ* absorbance monitoring with transmission electron microscopy observations. A correlation between the interfacial properties of the $TiO_2$ material in the presence of the different alcohol molecules and the photodeposition rate of platinum nanoparticles will be discussed.

## 2. EXPERIMENTAL SECTION

**2.1. $TiO_2$ Synthesis via Sol−Gel Process.** 2.96 mL of titanium isopropoxide is mixed with 20 mL of isopropanol. The mixture is brought to 0 °C in an ice bath. The solution is magnetically stirred prior to the addition of 10 mL of ultrapure water. The gel obtained is then filtered and dried in an oven at 60 °C overnight. The powder is then calcined at 400 °C for 2 h in air atmosphere.

**Received:** November 4, 2013
**Revised:** December 20, 2013
**Published:** December 20, 2013





dx.doi.org/10.1021/jp410846k | *J. Phys. Chem. C* 2014, 118, 1111−1117

**2.2. Powder X-ray Diffraction (XRD) Measurements.** XRD measurements of $TiO_2$ powders were carried out on an EMPYREAN PANALYTICAL. X-ray diffractometer using Cu K$\alpha$ radiation ($\lambda$ = 0.154 06 nm). The XRD spectra were obtained using high resolution with the step-scanning mode, a narrow receiving slit (1/16°), and a counting time of 240 s per 0.05°. Scans were recorded in the range of 20°−140°. The identification of the phases was made with reference to the Joint Committee on Powder Diffraction Standards International Center for Diffraction Data (JCPDS-ICDD) database.

**2.3. Transmission Electron Microscopy (TEM).** The morphology and size of particles were first examined with a TEM on a JEOL JEM-2001 equipped with a $LaB_6$ filament. The samples were characterized under an accelerating voltage of 200 kV and a resolution of ca. 0.19 nm.

**2.4. *In Situ* Absorbance Monitoring during the Photodeposition Process.** The photodeposition procedure was carried out as follows: 52.6 mg of $TiO_2$ (anatase), synthesized by the sol−gel technique, was mixed in argon-saturated 28 mL of water in a photoreactor provided with two optical quartz windows. The alcohol concentration was adjusted to 2 M in the photoreactor containing 34.7 mg of Pt salt ($H_2PtCl_6{\cdot}6H_2O$). The suspension was saturated with Ar and kept under constant stirring for 3 h. The source of ultraviolet (UV) and visible (Vis) radiation used for the experiments was a Xe lamp (159 W, ITS PS 150-9). In order to prevent the heating of the samples, the infrared (IR) photons were avoided using a hot mirror UV (Edmund Optics, F46507) and a water filter. A light detector (Rad Probe, LP 471) was fixed on top of the photoreactor to follow up the reaction kinetics. The detector used allows monitoring the absorbance changes in the 400−1050 nm spectral range. Therefore, a useful spectral range to follow up the rate of electron accumulation in the conduction band of $TiO_2$ leading to absorbance changes in the 700−800 nm.[24−28] The detector was connected to a photo/radiometer (Delta OHM HD 2102.2). The suspension containing the $TiO_2$ and $H_2O$ was used to record the irradiance at the beginning of the experiment, $A_0$. The light detector monitored the evolution of the irradiance, $A_1$, with time. The ratio $A_1/A_0$ was calculated to determine the absorbance.

**2.5. Photoelectrochemical Measurements.** *2.5.1. $TiO_2$ Photoelectrodes.* In brief, a suspension containing 10 mg of $TiO_2$ powder and 2 mL of ethanol was prepared. The mixture was ultrasonically stirred for 2 h to ensure an homogeneous dispersion; after that, 300 $\mu$L of suspension was sprayed via an airbrush over the conductive $SnO_2$:F (SOLEMS ASAHI 100) surface. The resistance of the glass is 70 Ω/sq. The deposit was allowed to dry for 15 min before calcination at 400 °C in air atmosphere for 2 h. The electric contact of the electrode was done by a copper wire in a region free of $TiO_2$ with silver epoxy (RS components).

*2.5.2. Photoelectrochemical Measurements.* Current−potential curves were measured in a photoelectrochemical cell provided with three-electrode compartment: working $TiO_2$ porous layer photoelectrode, a glassy carbon counter electrode, and a reversible hydrogen reference electrode. The photoelectrochemical measurements were carried out in an Ar-purged 0.5 M $K_2SO_4$ electrolyte under darkness and ultraviolet−visible radiation. A shutter was used during these experiments. All the aqueous solutions were prepared using 18.2 MΩ cm Millipore Milli-Q water. The cell set on an X-Y-Z axis drive metric stage plate (Edmund Optics 56-340) had a quartz window. A 150 W xenon lamp (Spectral Products ASB-XE-175) was used as a source of ultraviolet−visible illumination. The incident irradiance for the photoelectrode surface was 4.32 mW $cm^{-2}$.

## 3. RESULTS AND DISCUSSION

**3.1. Physical−Chemical Characterization of the Synthesized $TiO_2$ Material.** X-ray diffraction patterns were recorded in order to obtain information regarding the crystalline structure, the crystallite size, and microstrains affecting the $TiO_2$ sample. Figure 1 shows the X-ray diffraction spectrum of the heat-treated $TiO_2$ powder. All the diffraction peaks can be assigned to the tetragonal anatase crystalline phase of $TiO_2$. It can be furthermore mentioned that no additional peaks have been observed in addition to those assigned to the anatase phase which indicates high purity of the sample. The inset of Figure 1 shows the diffraction pattern recorded with the pristine sample. It appears that diffraction peaks corresponding to the anatase phase are broad and not well-defined. As a conclusion, the heat treatment allows transforming the disordered phase into a well-crystallized one. The specific surface area of the $TiO_2$ powder, determined by nitrogen adsorption experiments (data not shown), decreased from 280 $m^2\ g^{-1}$ down to 210 $m^2\ g^{-1}$.

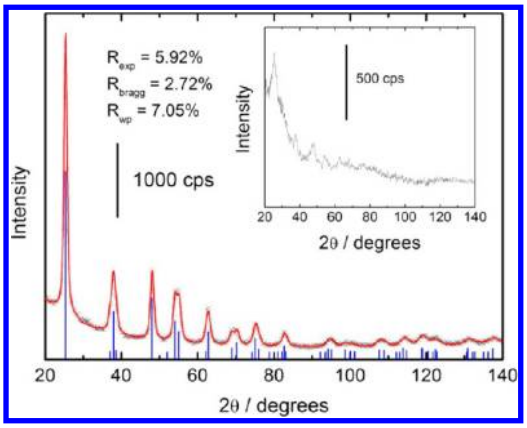


**Figure 1.** Rietveld refinement pattern of the heat-treated $TiO_2$ powder synthesized via the sol−gel process. Black dots represent the observed intensities, and the solid lines are calculated ones. Positions of Bragg peaks are marked with vertical blue bars. Rietveld agreement factors are given. The diffraction pattern obtained on the pristine powder is given in the inset.

Diffraction patterns were refined by using pseudo-Voigt functions using the Highscore Plus refinement program. The shape parameter $\eta$ is defined as the Lorentz fraction of the pseudo-Voigt function. The $K_{\alpha 2}$ component was taken into account by simultaneous fitting of two pseudo-Voigt functions for each diffraction peak. The starting atomic parameters for anatase ($I41/amd$ space group) were obtained from Howard et al.[29] The following parameters were refined: scale factor, zero point, background coefficients (a sixth-order polynomial function was used); unit cell parameters, profile coefficients, atomic positions, and isotropic displacement of titanium atoms. In each case, a good agreement between calculated and observed patterns was observed. The reliability factors were calculated according to relations given by Young.[30] As a result, the obtained lattice parameters from the fit were extracted and found to be equal to 3.786 and 9.494 Å, respectively.


dx.doi.org/10.1021/jp410846k | J. Phys. Chem. C 2014, 118, 1111−1117

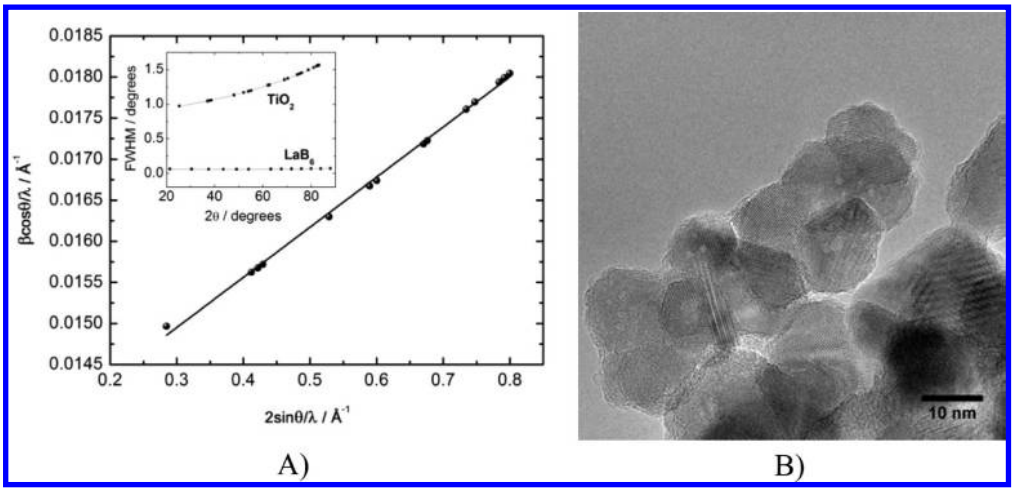


**Figure 2.** (A) Williamson–Hall plot obtained from XRD data recorded on $TiO_2$ powder synthesized via the sol–gel process. The evolution of the full width at half-maximum (fwhm) as a function of the diffraction angle is given in the inset graph for $TiO_2$ and $LaB_6$ standard. (B) TEM image of the $TiO_2$ nanoparticles.

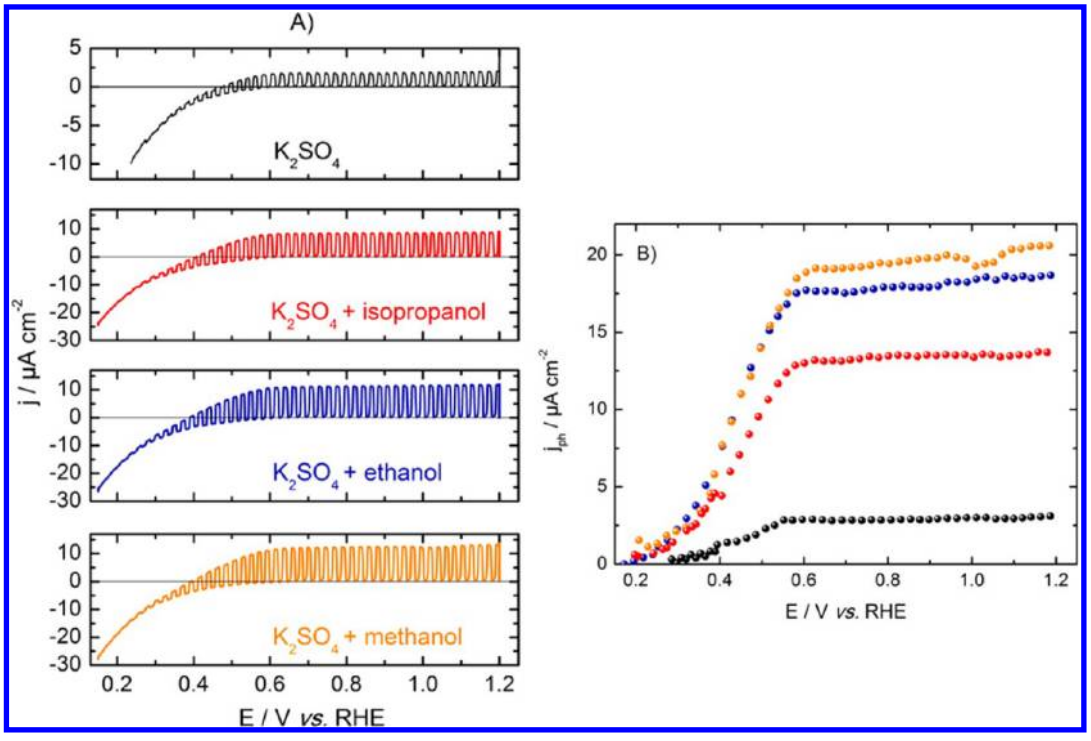


**Figure 3.** (A) Linear sweep photovoltammograms recorded with chopped irradiation of the $TiO_2$ photoelectrode in a $N_2$-purged electrolyte containing $K_2SO_4$ (0.5 M), $K_2SO_4$ (0.5 M) + isopropanol (0.1 M), $K_2SO_4$ (0.5 M) + ethanol (0.1 M), and $K_2SO_4$ (0.5 M) + methanol (0.1 M). (B) Extracted photocurrent response of the $TiO_2$ electrode prepared by sol–gel process in $N_2$-purged $K_2SO_4$ electrolyte in the presence of isopropanol (red dots), ethanol (blue dots), and methanol (orange dots) and in the absence of organics (dark dots). Scan rate 2 mV $s^{-1}$. The electrode geometric surface area is 1.59 $cm^2$.

Information concerning the microstructure of the sample (apparent crystallite size as well as microstrains) was extracted from the pattern by using line broadening analysis and classical Williamson–Hall plot. For each diffraction peak, the integral width of the Lorentzian and Gaussian components of the pseudo-Voigt function used for the fit are first determined according to the empirical formulas given by De Keijser et al.[31] After correcting the instrumental broadening using a $LaB_6$ standard powder, the integral width ($\beta$) of the function corresponding to a diffraction peak was calculated.[32] Finally a classical Williamson–Hall plot[33] was used in order to perform a microstructural analysis of the synthesized $TiO_2$ powder. The values of $\beta \cos(\theta)/\lambda$ were plotted against $2 \sin(\theta)/\lambda$, where $\theta$ is the Bragg angle and $\lambda$ the wavelength in angstroms. In agreement with the following relation, the reciprocal of the intercept gives an estimation of the size of coherently diffracting domains ($D_v$), while the slope provides information about microstrains ($\sigma$).

$$\beta = \frac{1}{D_v} + \frac{4\sigma \sin\theta}{\lambda} \quad (1)$$


dx.doi.org/10.1021/jp410846k | J. Phys. Chem. C 2014, 118, 1111–1117

Assuming that no anisotropic broadening can be associated with dislocations or stacking faults, the plot presented in Figure 2 provides qualitative information in relation to the microstructure of the sample.[34] The inset graph of Figure 2 confirms that the instrumental broadening is negligibly small in comparison with the sample broadening.

From the Williamson–Hall plot the apparent isotropic size of coherently diffracting domains, $D_v$, as well as the microstrain affecting the $TiO_2$ material have been found to be respectively equal to 7.6 nm and 0.3%. Assuming that particles are spherical, their mean diameter, $\langle d \rangle$, can be calculated from extracted XRD data as follows: $\langle d \rangle = {}^4/_3 D_v$ = 10.1 nm. This is in agreement with TEM observations (cf. Figure 2B).

**3.2. Photoelectrochemical Measurements in the Presence of Different Alcohol Molecules.** The photoelectrochemical performance of the $TiO_2$ nanomaterial in the presence of different alcohol molecules (ethanol, isopropanol, and methanol) is assessed using linear sweep voltammetry (cf. Figure 3A). The figure shows the typical photocurrent response under UV illumination of nanoporous $TiO_2$ photoelectrode in contact with an aqueous electrolyte. The rise and fall of the photocurrent value is associated with the illumination being chopped on and off. The different alcohol molecules act as hole acceptor capable of limiting losses due to electron–hole pair recombination. The observed photocurrent, in the absence of an organic molecule, is due to the oxygen evolution reaction.[35] When an organic molecule is added into the electrolyte, the photocurrent response is associated with the photooxidation of water and the organic molecule.[36,37] In each case it can be seen from Figure 3A that the presence of an organic molecule shifts the photocurrent onset potential toward negative values. These values are ca. 0.230, 0.193, 0.184, and 0.175 V vs RHE when no alcohol, isopropanol, ethanol, and methanol are respectively added in the electrolyte. These onset potential values were estimated by deriving the $j$–$E$ curves depicted in Figure 3A. The negative shift of the photocurrent onset potential is due to the ability of alcohol molecules to capture holes at the semiconductor surface more efficiently than hydroxyl ions in reason for the stronger adsorption strength of the alcohol molecules. The different onset potential values testify that the use of alcohol molecules as hole scavengers allows inhibiting the electron–hole pair recombination near the flat-band position.

Figure 3B shows the evolution of the photocurrent density ($j_{ph}$) as a function of the applied electrode potential. The photocurrent value was calculated by subtracting the dark current from the current measured in the presence of light. For all investigated alcohols, the photocurrent measured at the $TiO_2$ electrode increases before leveling off. The potential at which the photocurrent levels off or saturates depends on the alkyl chain length of the alcohol molecule used as hole acceptor. At potential near the flat-band potential, it can be noticed that the photocurrent response increases faster when alcohol molecules are added into the electrolyte. Its rate of increase in the presence of different hole acceptors follows the order $H_2O$ < isopropanol < ethanol ≈ methanol. At applied electrode potential >0.6 V/RHE, the number of holes or the concentration of organics at the interface can clearly explain the observed saturated photocurrent. The magnitude of the photocurrent plateau follows the order methanol ≈ ethanol > isopropanol > $H_2O$ with ratios with respect to $H_2O$ of 6.4, 5.8, and 4.3, respectively. All investigated alcohols possess $\alpha$-hydrogen atoms and can consequently react as current doubling reagents.[38,39] Consequently, the observed differences in the photocurrent response using dissimilar alcohol molecules result in their different adsorption strength at the $TiO_2$ surface. However, the magnitude of the photocurrent response obtained in the presence of the different alcohol molecules exceeds what is predicted by the phenomenon known as current doubling effect.[40] This unusual high response was observed by Wahl et al.[41] with a 20-fold increase of the photocurrent value in the presence of methanol over that observed for the supporting electrolyte alone. Herein the investigated electrode possesses a porous film with particles (ca. 10.1 nm) surrounded by the electrolyte. These facts imply that no space charge region is developed, and as a conclusion, the charge separation is governed by the process of charge transfer at the particle/electrolyte interface.[42,43] The reason for the unusual high photocurrent response was suggested by Poznyak et al.[44] and seems to be the result of the oxidation of the hole acceptor which hinders the photogeneration of oxygen. Oxygen is a good scavenger for photogenerated electrons, preventing them from reaching the electrode back-contact[45] and thus decreasing the photocurrent response.

**3.3. *In Situ* Monitoring of the Photodeposition Process in the Presence of Different Alcohol Molecules.** The photodeposition kinetics was monitored *in situ* by measuring the evolution of the absorbance of the solution in the 400–1050 nm spectral range as a function of time. For each organics used as hole scavenger, TEM experiments were carried out at different deposition times in order to follow the growth rate of platinum particles (see Figure 4).

*3.3.1. Effect of the Hole Scavenger on the Photodeposition Process.* Whatever the organics added into the

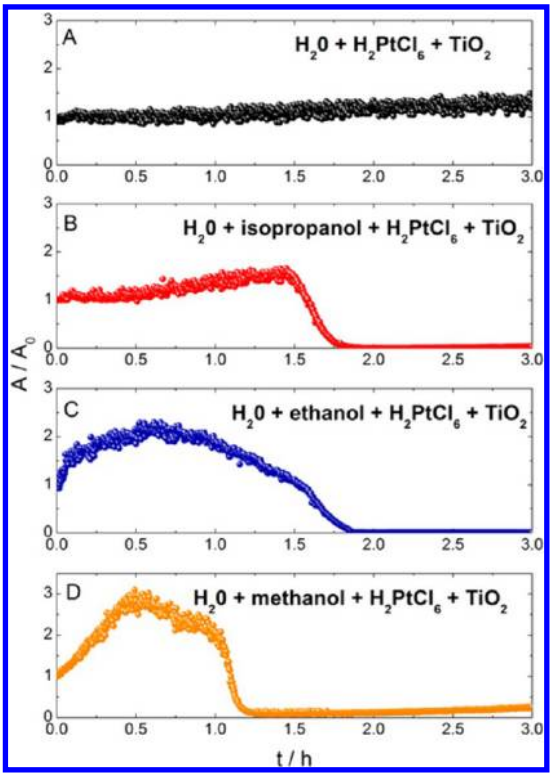


**Figure 4.** *In situ* monitoring of the evolution of the absorbance of the solution during the photodeposition process in the absence of alcohols (A) and in the presence of isopropanol (B), ethanol (C), and methanol (D). The alcohol concentration was 2 M.


dx.doi.org/10.1021/jp410846k | J. Phys. Chem. C 2014, 118, 1111–1117

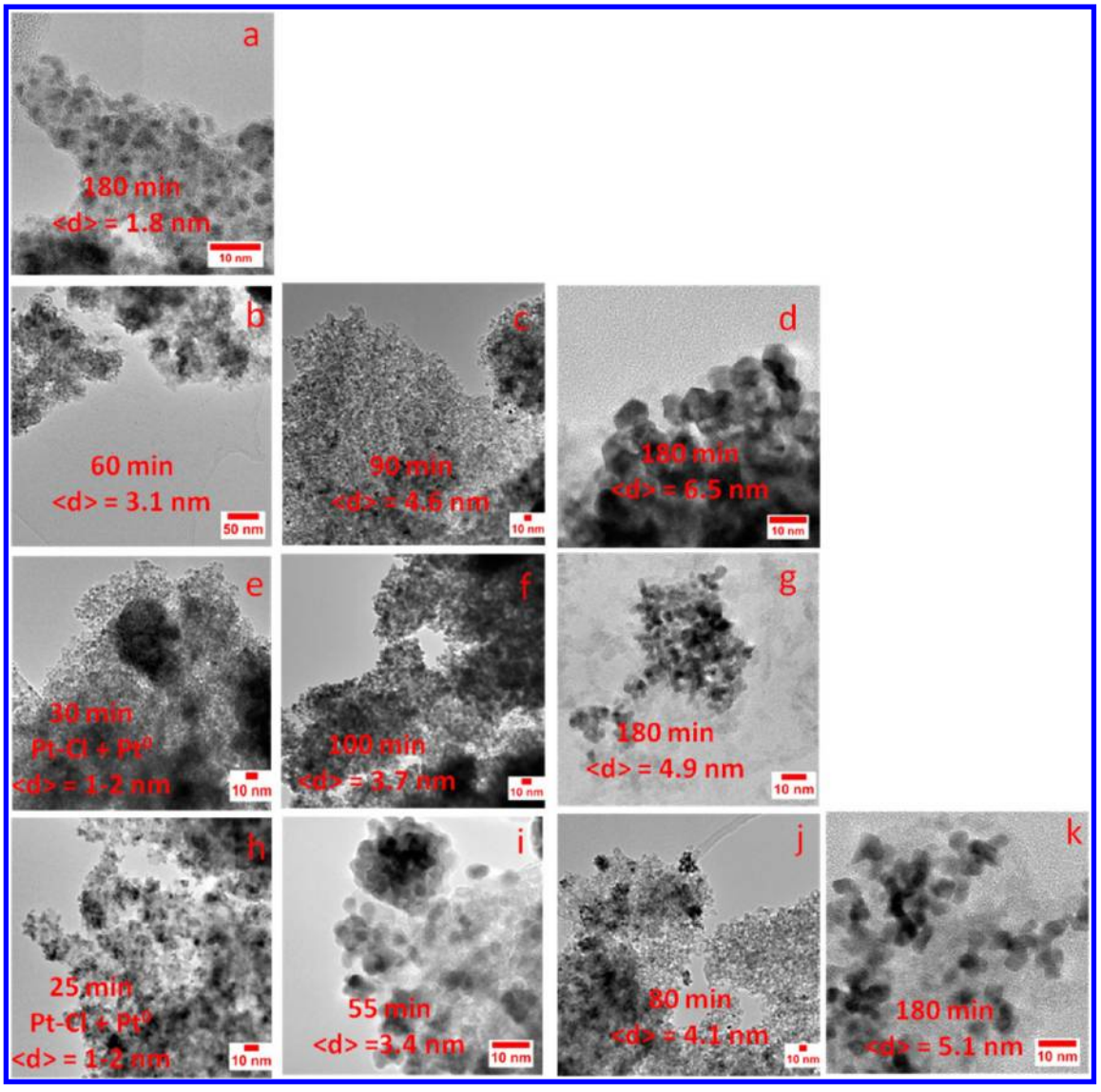


**Figure 5.** TEM images recorded at different deposition times during the photodeposition process of Pt nanoparticles onto nanoparticulated oxide anatase phase substrate in the presence of water (a), isopropanol (b–d), ethanol (e–g), and methanol (h–k). In each case an estimation of the mean particle size is given. The standard deviation is estimated to be 0.5 nm.

electrolyte, the absorbance of the solution first increases before reaching a saturation point and then decreases. In the initial stage the rate of increase of the absorbance as a function of time strongly depends on the chemical nature of the hole scavenger used. This increase of absorbance can be associated with the accumulation of electrons in the conduction band of $TiO_2$. It has in fact already been confirmed by several groups[24−28] that the UV-light illumination of a $TiO_2$ nanopowder, immersed in aqueous electrolyte, could lead to an increase of absorbance in the 700−800 nm spectral range associated with a change of the color of the $TiO_2$ particles. This electron accumulation is due to the formation, as intermediate, of a radical species ($RO^{\bullet}$), which is able to inject an electron into the conduction band of $TiO_2$. Therefore, the increase in absorbance at this initial stage can be associated with the presence of alcohols which are able to promote the accumulation of electrons at the $TiO_2$ conduction band. It was furthermore reported that the increase in the absorbance only occurs in the presence of $TiO_2$ in the electrolyte.[46] The rate of absorbance increase in the presence of the different alcohols follows the order methanol ≈ ethanol > isopropanol > $H_2O$. This behavior can be fully correlated with the magnitude of the photocurrent response observed in the presence of different alcohol molecules and seems consequently related to the adsorption strength of the alcohol at the $TiO_2$ surface. TEM images presented in Figure 5 show that the reduction of platinum complex into agglomerated metallic clusters begins to occur during the initial stage of the photodeposition process. It is most probable that the rate of nucleation events is related to the rate of absorbance increase in the presence of the different alcohols. The nucleation step is followed by the growth step. Once small nuclei are formed during the initial stage, the development of clusters occurs through a slow surface-growth mechanism. However, whatever the organics used the metal ions photoreduction is not completed since the presence of the chemical precursor was evidenced by energy-dispersive X-ray spectrometry (data not shown). At this stage, platinum clusters are uniform in size when methanol, ethanol, or isopropanol is used as hole scavenger (Figure 5b,e,h).


dx.doi.org/10.1021/jp410846k | J. Phys. Chem. C 2014, 118, 1111−1117

The presence of organics in the solution induces an increase in the absorbance, reaching a maximum point (Figure 4). This latter is not attained in the absence of organics even after irradiating the solution for 3 h (Figure 4A). The time at which the maximum of absorbance is obtained, and its value strongly depends on the nature of the hole scavenger used. At this situation the surface of $TiO_2$ particles is covered by platinum metallic clusters. Most of the generated electron−hole pairs recombine. Thereafter, the decrease of the absorbance can be associated with the electron−hole pair recombination, the diminution of the platinum complex in the solution, and the absorption of light by the platinum clusters formed. After this situation, an autocatalytic process might explain the slight increase of the mean particle size observed, whatever the hole scavenger used (Figure 5c,d, Figure 5f,g, Figure 5i−k). Under these experimental conditions (cf. Figures 4 and 5), a complete reduction of the metallic precursor for reduction times of ca. 75, 110, and 105 min when methanol, ethanol, and isopropanol are respectively used as hole scavenger can be deduced. On the other hand, when water is used as hole scavenger, an irradiation time of 180 min is not enough to completely reduce the metallic precursor, as testified by TEM observations and energy-dispersive X-ray spectrometry. In this case, though, the number of nucleation sites is low; in reason for the weak electron accumulation at the $TiO_2$ conduction band, the noncomplete reduction of the metal precursor coupled with the slow surface growth of platinum clusters favors a low mean particle size (i.e., 1.8 nm). Additionally, platinum nanoparticles are well-dispersed contrary to nanoparticles deposited in the presence of alcohol molecules. This opens an interesting way to control the size and dispersion of photodeposited platinum nanoparticles by using a fully green chemistry approach. The final size of platinum nanoparticles is respectively of ca. 4.9, 5.1, and 6.5 nm in the presence of methanol (Figure 5k), ethanol (Figure 5g), and isopropanol (Figure 5d), respectively. Therefore, particles of platinum >2 nm are generated in the presence of isopropanol. This may be explained by the formation of a weaker number of nuclei during the initial stage of the photodeposition process. Summing up, the results obtained herein allow envisioning promising ways to control the size and shape of photodeposited noble-metal-based nanoparticles onto semiconductor oxides. These factors must be taken into account: the reduction time, the chemical nature of the hole scavenger used, and the nature of the oxide surface.

## 4. CONCLUSIONS

In this work, the photocurrent response of $TiO_2$ nanoparticles synthesized via the sol−gel process was investigated in the presence of different alcohols (methanol, ethanol, isopropanol). The nanocrystalline $TiO_2$ photoelectrode enhanced the photocurrent in the presence of alcohol molecules. The magnitude of the photocurrent response was a function of the nature of the alcohol used. It followed the order methanol ≈ ethanol > isopropanol > $H_2O$. By measuring the irradiance of transmitted visible light through a solution with the reactants, we were able to monitor, in real time, the photodeposition process of platinum nanoclusters on $TiO_2$ particles in the presence of different alcohol molecules. At the initial stage of the photodeposition process, the rate increase of absorbance in the presence of the different alcohols follows the order methanol ≈ ethanol > isopropanol > $H_2O$. This behavior was correlated with the magnitude of the photocurrent response observed in the presence of different alcohol molecules and seems to be related to the adsorption strength of the alcohol at the $TiO_2$ surface. Furthermore, this study opens interesting perspectives concerning the control of the size of photodeposited platinum nanoparticles. Additionally, a modification of platinum surface facets can be achieved by using isopropanol as hole scavenger. This study thus allows envisioning future developments concerning plasmonic photocatalysis research domain where the size and shape of the catalyst plays an essential role.

## AUTHOR INFORMATION


### Corresponding Authors

*E-mail aurelien.habrioux@univ-poitiers.fr (A.H.).
*E-mail nicolas.alonso.vante@univ-poitiers.fr (N.A.-V.).

### Present Addresses

A.S.G.: Institute of Technical Thermodynamics/Electrochemical Energy Technology, German Aerospace Center (DLR), Pfaffenwaldring 38-40, 70569 Stuttgart, Germany.
E.V.: Facultad de Ingeniería UABC Mexicali, Blvd. Benito Juárez y calle de la Normal s/n, Col. Insurgentes Este, C.P. 21280, México.


### Notes

The authors declare no competing financial interest.

## ACKNOWLEDGMENTS

J. Ma thanks the Ministère de l'Enseignement Supérieur et de la Recherche for a fellowship and Poitou-Charentes region for financial support. E. Valenzuela acknowledges the CCIIA-UABC for the financial support provided through the program "Apoyo a la Movilidad Académica 2013".

## REFERENCES


(1) Atyaoui, A.; Bousselmi, L.; Cachet, H.; Pu, P.; Sutter, E. M. M. Influence of Geometric and Electronic Characteristics of $TiO_2$ Electrodes with Nanotubular Array on Their Photocatalytic Efficiencies. *J. Photochem. Photobiol. A: Chem.* **2011**, *224*, 71−79.

(2) Hagfeldt, A.; Graetzel, M. Light-Induced Redox Reactions in Nanocrystalline Systems. *Chem. Rev.* **1995**, *95*, 49−68.

(3) Cahen, D.; Hodes, G.; Grätzel, M.; Guillemoles, J. F.; Riess, I. Nature of Photovoltaic Action in Dye-Sensitized Solar Cells. *J. Phys. Chem. B* **2000**, *104*, 2053−2059.

(4) Heintz, O.; Robert, D.; Weber, J. V. Comparison of the Degradation of Benzamide and Acetic Acid on Different $TiO_2$ Photocatalysts. *J. Photochem. Photobiol. A: Chem.* **2000**, *135*, 77−80.

(5) Gao, F. G.; Bard, A. J.; Kispert, L. D. Photocurrent Generated on a Carotenoid-Sensitized $TiO_2$ Nanocrystalline Mesoporous Electrode. *J. Photochem. Photobiol. A: Chem.* **2000**, *130*, 49−56.

(6) Bamwenda, G. R.; Tsubota, S.; Nakamura, T.; Haruta, M. The Influence of the Preparation Methods on the Catalytic Activity of Platinum and Gold Supported on $TiO_2$ for CO Oxidation. *Catal. Lett.* **1997**, *44*, 83−87.

(7) Timperman, L.; Feng, Y. J.; Vogel, W.; Alonso-Vante, N. Substrate Effect on Oxygen Reduction Electrocatalysis. *Electrochim. Acta* **2010**, *55*, 7558−7563.

(8) Timperman, L.; Gago, A. S.; Alonso-Vante, N. Oxygen Reduction Reaction Increased Tolerance and Fuel Cell Performance of Pt and $Ru_xSe_y$ onto Oxide−Carbon Composites. *J. Power Sources* **2011**, *196*, 4290−4297.

(9) Ruiz Camacho, B.; Morais, C.; Valenzuela, M. A.; Alonso-Vante, N. Enhancing Oxygen Reduction Reaction Activity and Stability of Platinum via Oxide-Carbon Composites. *Catal. Today* **2013**, *202*, 36−43.

(10) Ma, J.; Habrioux, A.; Pisarek, M.; Lewera, A.; Alonso-Vante, N. Induced Electronic Modification of Pt Nanoparticles Deposited onto

Graphitic Domains of Carbon Materials by UV Irradiation. *Electrochem. Commun.* **2013**, *29*, 12−16.
(11) Sugimura, H.; Uchida, T.; Kitamura, N.; Masuhara, H. Photocatalytic Micropatterning of Titanium Oxide Surface with Platinum. *Chem. Lett.* **1993**, *22*, 379−382.
(12) Vogel, W.; Timperman, L.; Alonso-Vante, N. Probing Metal Substrate Interaction of Pt Nanoparticles: Structural XRD Analysis and Oxygen Reduction Reaction. *Appl. Catal., A* **2010**, *377*, 167−173.
(13) Lewera, A.; Timperman, L.; Roguska, A.; Alonso-Vante, N. Metal−Support Interactions between Nanosized Pt and Metal Oxides ($WO_3$ and $TiO_2$) Studied Using X-Ray Photoelectron Spectroscopy. *J. Phys. Chem. C* **2011**, *115*, 20153−20159.
(14) Chen, C.-S.; Pan, F.-M. Electrocatalytic Activity of Pt Nanoparticles Deposited on Porous $TiO_2$ Supports toward Methanol Oxidation. *Appl. Catal., B* **2009**, *91*, 663−669.
(15) Shkrob, I. A.; Sauer, M. C. Hole Scavenging and Photo-Stimulated Recombination of Electron−Hole Pairs in Aqueous $TiO_2$ Nanoparticles. *J. Phys. Chem. B* **2004**, *108*, 12497−12511.
(16) Kraeutler, B.; Bard, A. J. Heterogeneous Photocatalytic Preparation of Supported Catalysts. Photodeposition of Platinum on Titanium Dioxide Powder and Other Substrates. *J. Am. Chem. Soc.* **1978**, *100*, 4317−4318.
(17) Vorontsov, A. V.; Savinov, E. N.; Zhensheng, J. Influence of the Form of Photodeposited Platinum on Titania Upon Its Photocatalytic Activity in CO and Acetone Oxidation. *J. Photochem. Photobiol. A: Chem.* **1999**, *125*, 113−117.
(18) Chanjuan, X.; Zhengshi, C.; Qinglin, L.; Zhensheng, J. Effects of $H^+$, $Cl^-$ and $CH_3COOH$ on the Photocatalytic Conversion of $PtCl_6^{2-}$ in Aqueous $TiO_2$ Dispersion. *J. Photochem. Photobiol. A: Chem.* **1995**, *87*, 249−255.
(19) Jin, Z.; Chen, Z.; Li, Q.; Xi, C.; Zheng, X. On the Conditions and Mechanism of $PtO_2$ Formation in the Photoinduced Conversion of $H_2PtCl_6$. *J. Photochem. Photobiol. A: Chem.* **1994**, *81*, 177−182.
(20) Zhang, F.; Chen, J.; Zhang, X.; Gao, W.; Jin, R.; Guan, N.; Li, Y. Synthesis of Titania-Supported Platinum Catalyst: The Effect of pH on Morphology Control and Valence State during Photodeposition. *Langmuir* **2004**, *20*, 9329−9334.
(21) Teramura, K.; Okuoka, S.-i.; Yamazoe, S.; Kato, K.; Shishido, T.; Tanaka, T. In Situ Time-Resolved Energy-Dispersive Xafs Study on Photodeposition of Rh Particles on a $TiO_2$ Photocatalyst. *J. Phys. Chem. C* **2008**, *112*, 8495−8498.
(22) Ismail, A. A.; Al-Sayari, S. A.; Bahnemann, D. W. Photodeposition of Precious Metals onto Mesoporous $TiO_2$ Nanocrystals with Enhanced Their Photocatalytic Activity for Methanol Oxidation. *Catal. Today* **2013**, *209*, 2−7.
(23) Maicu, M.; Hidalgo, M. C.; Colón, G.; Navío, J. A. Comparative Study of the Photodeposition of Pt, Au and Pd on Pre-Sulfated $TiO_2$ for the Photocatalytic Decomposition of Phenol. *J. Photochem. Photobiol. A: Chem.* **2011**, *217*, 275−283.
(24) Boschloo, G.; Fitzmaurice, D. Electron Accumulation in Nanostructured $TiO_2$ (Anatase) Electrodes. *J. Phys. Chem. B* **1999**, *103*, 7860−7868.
(25) Freemantle, R. G.; Guo, W.; Liu, M.; Obare, S. O. One-Step Synthetic Procedures and Electrochemical Properties of Monodisperse 1−2 nm Metallic Nanoparticles. *ECS Trans.* **2007**, *6*, 93−99.
(26) Serpone, N.; Lawless, D.; Khairutdinov, R. Size Effects on the Photophysical Properties of Colloidal Anatase $TiO_2$ Particles: Size Quantization Versus Direct Transitions in This Indirect Semiconductor? *J. Phys. Chem.* **1995**, *99*, 16646−16654.
(27) Kamat, P. V.; Bedja, I.; Hotchandani, S. Photoinduced Charge Transfer between Carbon and Semiconductor Clusters. One-Electron Reduction of $C_{60}$ in Colloidal $TiO_2$ Semiconductor Suspensions. *J. Phys. Chem.* **1994**, *98*, 9137−9142.
(28) Gopidas, K. R.; Bohorquez, M.; Kamat, P. V. Photophysical and Photochemical Aspects of Coupled Semiconductors: Charge-Transfer Processes in Colloidal Cadmium Sulfide-Titania and Cadmium Sulfide-Silver(I) Iodide Systems. *J. Phys. Chem.* **1990**, *94*, 6435−6440.
(29) Howard, C. J.; Sabine, T. M.; Dickson, F. Structural and Thermal Parameters for Rutile and Anatase. *Acta Crystallogr., Sect. B* **1991**, *47*, 462−468.
(30) Young, R. A. *Introduction to the Rietveld Method*; Oxford University Press: Oxford, 1993.
(31) de Keijser, T.; Mittemeijer, E. J.; Rozendaal, H. C. F. The Determination of Crystallite-Size and Lattice-Strain Parameters in Conjunction with the Profile-Refinement Method for the Determination of Crystal Structures. *J. Appl. Crystallogr.* **1983**, *16*, 309−316.
(32) de Keijser, T. H.; Langford, J. I.; Mittemeijer, E. J.; Vogels, A. B. P. Use of the Voigt Function in a Single-Line Method for the Analysis of X-Ray Diffraction Line Broadening. *J. Appl. Crystallogr.* **1982**, *15*, 308−314.
(33) Williamson, G. K.; Hall, W. H. X-Ray Line Broadening from Filed Aluminium and Wolfram. *Acta Metall.* **1953**, *1*, 22−31.
(34) Tobaldi, D. M.; Pullar, R. C.; Gualtieri, A. F.; Seabra, M. P.; Labrincha, J. A. Phase Composition, Crystal Structure and Microstructure of Silver and Tungsten Doped $TiO_2$ Nanopowders with Tuneable Photochromic Behaviour. *Acta Mater.* **2013**, *61*, 5571−5585.
(35) Bogdanoff, P.; Alonso-Vante, N. On-Line Determination via Differential Electrochemical Mass Spectroscopy (DEMS) of Chemical Products Formed in Photoelectrocatalytic Systems. *Ber. Bunsen-Ges. Phys. Chem.* **1993**, *97*, 940−942.
(36) Bogdanoff, P.; Alonso-Vante, N. A Kinetic Approach of Competitive Photoelectrooxidation of Hcooh and $H_2O$ on $TiO_2$ Anatase Thin Layers via On-Line Mass Detection. *J. Electroanal. Chem.* **1994**, *379*, 415−421.
(37) Lana Villarreal, T.; Gomez, R.; Neumann-Spallart, M.; Alonso-Vante, N.; Salvador, P. Semiconductor Photooxidation of Pollutants Dissolved in Water: A Kinetic Model for Distinguishing between Direct and Indirect Interfacial Hole Transfer. I. Photoelectrochemical Experiments with Polycrystalline Anatase Electrodes under Current Doubling and Absence of Recombination. *J. Phys. Chem. B* **2004**, *108*, 15172−15181.
(38) Miyake, M.; Yoneyama, H.; Tamura, H. Two Step Oxidation Reactions of Acohols on an Illuminated Rutile Electrode. *Chem. Lett.* **1976**, *5*, 635−640.
(39) Yamagata, S.; Nakabayashi, S.; Sancier, K. M.; Fujishima, A. Photocatalytic Oxidation of Alcohols on $TiO_2$. *Bull. Chem. Soc. Jpn.* **1988**, *61*, 3429−3434.
(40) Hykaway, N.; Sears, W. M.; Morisaki, H.; Morrison, S. R. Current-Doubling Reactions on Titanium Dioxide Photoanodes. *J. Phys. Chem.* **1986**, *90*, 6663−6667.
(41) Wahl, A.; Ulmann, M.; Carroy, A.; Augustynski, J. Highly Selective Photo-Oxidation Reactions at Nanocrystalline $TiO_2$ Film Electrodes. *J. Chem. Soc., Chem. Commun.* **1994**, 2277−2278.
(42) Fabregat-Santiago, F.; Garcia-Belmonte, G.; Bisquert, J.; Zaban, A.; Salvador, P. Decoupling of Transport, Charge Storage, and Interfacial Charge Transfer in the Nanocrystalline $TiO_2$/Electrolyte System by Impedance Methods. *J. Phys. Chem. B* **2001**, *106*, 334−339.
(43) Bisquert, J. Chemical Capacitance of Nanostructured Semiconductors: Its Origin and Significance for Nanocomposite Solar Cells. *Phys. Chem. Chem. Phys.* **2003**, *5*, 5360−5364.
(44) Poznyak, S. K.; Kokorin, A. I.; Kulak, A. I. Effect of Electron and Hole Acceptors on the Photoelectrochemical Behaviour of Nanocrystalline Microporous $TiO_2$ Electrodes. *J. Electroanal. Chem.* **1998**, *442*, 99−105.
(45) Byrne, J. A.; Eggins, B. R. Photoelectrochemistry of Oxalate on Particulate $TiO_2$ Electrodes. *J. Electroanal. Chem.* **1998**, *457*, 61−72.
(46) Ma, J.; Habrioux, A.; Alonso-Vante, N. Enhanced HER and ORR Behavior on Photodeposited Pt Nanoparticles onto Oxide−Carbon Composite. *J. Solid State Electrochem.* **2013**, *17*, 1913−1921.